Theoretical Studies on the UO_2^{2+} and Sr^{2+} Complexation by Phosphoryl-Containing $O{=}PR_3$ Ligands: QM ab Initio Calculations in the Gas Phase and MD FEP Calculations in Aqueous Solution

F. Hutschka, A. Dedieu,* L. Troxler, and G. Wipff*

UMR 7551, Institut de Chimie, Université Louis Pasteur, 4, rue Bloise Pascal, 67 000 Strasbourg, France

Received: December 9, 1997; In Final Form: February 27, 1998

We report a series of ab initio QM calculations on uranyl and Sr^{2+} complexes of $O{=}PR_3$ ligands (R = H Me Ph) to assess the role of substituents R and of NO_3^- counterions on the intrinsic cation−ligand interaction energy. When there are no counterions, the binding sequence of UO_2^{2+} and of Sr^{2+} complexes follows the order R = H < Me < Ph, due to polarization and charge-transfer effects. However, in the presence of NO_3^- counterions, the $OPMe_3$ and $OPPh_3$ complexes become of similar stability, due to the ligand−anion repulsive interactions. Complexes of OPR_3 with the spherical Sr^{2+} cation are found to be less stable than those with the linear UO_2^{2+} cation. In the second part of the paper we report molecular dynamics simulations in water on 1:1 and 2:1 complexes of OPR_3 with $UO_2(NO_3)_2$. The changes in free energies of solvation upon electronic reorganization of the ligand and $UO_2(NO_3)_2$ induced by complexation are investigated using statistical perturbation FEP techniques and found to be nearly independent of R. The importance of these results in the context of designing efficient ionophores for uranyl cations is discussed.

Introduction

The search for complexant molecules which specifically bind actinides and separate them from other cations represents a challenging task in the context of nuclear waste separation techniques and from a basic point of view.[1,2] The elementary interactions between the cation and the binding sites of the ligand are of major importance for the binding strength and selectivity.[3,4] In contrast with the large amount of theoretical and experimental data on alkali cations M^+,[5] those dealing with actinides and lanthanides are rather scarce. Concerning the uranyl cation, there are quantum mechanical studies on the bare ion[6−9] or its $UO_2(NO_3)_2$ and UO_2SO_4 salts,[7] and molecular dynamics simulations on the free and complexed ion in solution.[10−13] This led us to undertake systematic theoretical studies of these interactions, with various ions and ligands. In this paper, we focus on the uranyl cation UO_2^{2+} interacting with phosphoryl O═P binding sites. The latter are binding fragments of extractant molecules such as TBP (tributyl phosphate), CMPO, and phosphine oxides used experimentally (TRUEX process[14,15]) to extract lanthanides from nuclear wastes selectively, but so far, the question of their intrinsic interactions with actinides or lanthanides cations has not been elucidated.

Here, we first report a quantum mechanical (QM) study of UO_2^{2+} complexes with small model $O{=}PR_3$ ligands (R = H, methyl, phenyl) in order to compare their precise structures and intrinsic (gas phase) interaction energies as a function of R. With the smallest system (OPH_3 complex), several methodological investigations are performed concerning the basis set and the level of calculation. We then assess the role of counterions on the $UO_2^{2+}\cdots OPR_3$ interactions in the 1:1 complexes (R = H, Me, Ph). The NO_3^- anion was selected as counterion, because of the many related structural data[16] and because it is present in high concentrations in liquid solutions of nuclear wastes.[15] With the OPH_3 and $OPMe_3$ complexes, the 1:1 and 2:1 stoichiometries are considered. On the basis of these QM studies, the atomic charges on the different moieties of the complexes are calculated and discussed.

To compare the intrinsic binding features of the linear UO_2^{2+} with those of a spherical divalent cation we also simulated the $Sr^{2+}\cdots OPR_3$ and $Sr(NO_3)_2\cdots OPR_3$ 1:1 complexes, as Sr^{2+} is also potentially present in nuclear waste.

In addition to intrinsic binding features, solvation strongly contributes to the stability, nature, and binding selectivity of the complexes.[17,18] We therefore decided to simulate these complexes in aqueous solution to characterize their solvation features and stability. Water was chosen as a solvent, first to represent the source phase in extraction experiments, where the cation uptake by the ligand may take place. Second, the organic receiving phase is saturated with water, whose local concentration around the polar solute may be quite high. Water is also a strong competitor with ligand−cation binding. From the computational point of view, the direct calculation of absolute free energies of solvation would be presently untractable for large systems, but *differences* in free energies of solvation can be obtained more easily when the systems formally transform one into the other via small perturbations. As the ligand binds to a cation, there is some electron transfer to the latter, while the ligand becomes polarized. This electronic reorganization (ER) can be viewed as a series of small perturbations from the free to the complexed state, and the related change in solvation energy can be calculated using statistical perturbation techniques. Our goal in doing so was to assess the magnitude of this solvation effect as a function of the R substituent, compared to the change in intrinsic binding interactions. It could be indeed anticipated that the ligand which becomes the most polarized upon complexation also becomes the best hydrated and that changes in solvation could therefore contribute to the ion extraction selectivity.

Another of the motivations of our study was the so-called "anomalous aryl effect" (AAE) reported with bidentate phos-

S1089-5639(98)00469-1 CCC: $15.00
Published on Web 05/06/1998

phoryl containing ligands.[1] The AAE can be summarized as follows. In the case of neutral monodentate extractants, the extraction ability is reduced if the electronegativity of substituents adjacent to the P═O binding site increases, as expected from the electron withdrawal by the oxygen atom. However, with potentially bidendate diphosphine dioxides and CMPOs extractant molecules, replacement of alkyl by electron-withdrawing phenyl or tosyl groups enhances, instead of reducing, the extraction of Am^{3+} or of UO_2^{2+}.[1] This "aryl effect" is very useful for the extraction of actinides from nuclear waste, but is not clearly understood. For instance, the recently synthesized CMPO-calixarenes with O═P(phenyl)$_2$ moieties efficiently extract actinides and lanthanides, whereas the O═P(alkyl)$_2$ analogues do not.[19] This is why we compare $OPMe_3$/$OPPhe_3$ as model ligands to investigate the alkyl/aryl substituent effect.

Methods

The QM ab initio calculations were performed at the SCF and MP2 levels using the Gaussian-92 package.[20] The U atom is described as in ref 7 by the effective relativistic one-electron pseudopotential of Hay[21] for the 78 core electrons, corresponding to the [Xe]4f^{14}5d^{10} configuration of the Pt atom. The valence (5f,6d,7s) and semicore (6s,6p) orbitals of U are described by a [3s 3p 2d 2f] contracted Gaussian basis set. The explicit consideration of the semicore electrons (6s and 6p) in addition to the valence electrons should allow a correct treatment of the correlation effects at the MP_2 level.[22] One may of course worry about the non explicit representation of 5s, 5p, and 5d electrons. Calculations by Pyykkö et al.[23] carried out for UO_2^{2+} with either the 78-core-electron pseudopotential of Hay used here or the 60-core electron pseudopotential of Küchle et al.,[24] in conjunction with a larger basis set for U and O, yielded at the HF level U−O bond length values that are close to each other (1.673 and 1.660 Å, respectively). Very recent CCSD calculations carried out with the 60-core-electron pseudopotential yield a slighly greater value (1.697 Å). As we mostly focus on differences in binding properties within a series of ligands, our representation should be reasonable.

In our standard calculations, the Dunning double-ζ basis set was used for H, C, N, O, and P, with one set of 3d polarization functions on the P atom ($\zeta_{3d} = 0.37$). This basis is referred to as DZP*. In additional test calculations on the $UO_2(NO_3)_2$ OPR_3 complexes, polarization functions were added on "all" atoms (excepted on uranium) (i.e., the H (ζ_{2p}= 0.8), C ($\zeta_{3d} = 0.75$), N ($\zeta_{3d} = 0.8$), O ($\zeta_{3d} = 0.85$) atoms). This basis set is hereafter referred to as the DZA* basis set.

The geometry optimization was carried out as follows. The free ligands OPH_3, $OPMe_3$, and $OPPh_3$ were first optimized using analytical gradients. For $OPPh_3$, a pseudo C_s symmetry was assumed for the OPC_3 fragment, while the phenyl rings were allowed to rotate around the P−C bonds. For the optimizations of the systems involving UO_2^{2+}, a numerical gradient was used. The $UO_2(NO_3)_2$ salt was optimized under a D_{2h} symmetry constraint, according to the experimental geometries of $UO_2(NO_3)_2(H_2O)_2$ [25] or $UO_2(NO_3)_2(H_2O)_6$.[26] The $[UO_2\cdots OPR_3]^{2+}$ and $UO_2(NO_3)_2\cdots OPPh_3$ systems were optimized using the following constraints: C_s symmetry for R = H and Me ($\gamma = 0°$; see Figure 1), pseudo C_s symmetry for R = Ph as in $OPPh_3$ (i.e., allowing again the rotation of the phenyl rings), collinear arrangement of the O═U═O atoms of the uranyl and of the P═O···U atoms ($\alpha = 180°$; see Figure 1). For R = Ph, additional constraints were imposed: in $[UO_2\cdots OPPh_3]^{2+}$ the geometry of the phenyl ring was constrained to be the same as that in the optimized $OPPh_3$ ligand, and only the P−C, the P═O distances, the O−P−C angles, and the rotation angle around the P−C bond were optimized. In the $[UO_2(NO_3)_2\cdots OPPh_3]$ system, only the P═O distance and the rotation around the P−C bond were allowed to vary and the other geometrical parameters were kept as in $[UO_2\cdots OPPh_3]^{2+}$. Similarly, the geometry of the two NO_3^- groups was kept as in $[UO_2(NO_3)_2\cdots OPMe_3]$ and only the U···N distance was allowed to vary. For the Sr^{2+} complexes, constraints analogous to the ones described above for the UO_2^{2+} systems were used.

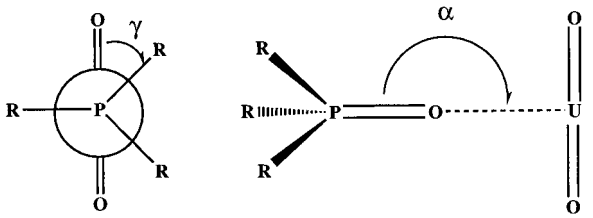

Figure 1. Schematic representation of the $UO_2^{2+}\cdots OPR_3$ complexes (R = H/Me/Ph)

The interaction energies between OPR_3 and the cation (in the complexes without counterion) or the $UO_2(NO_3)_2$ salt (in the presence of counterions) were calculated in the optimized complexes, and corrected for basis set superposition errors ("BSSE") using the counterpoise method.[27] As shown below, this correction turned out to be nearly constant in the series R = H/Me/Ph for the 1:1 complexes with UO_2^{2+}, Sr^{2+}, or $UO_2(NO_3)_2$. Since we are mostly interested in the assessment of energy *variations*, the BSSE was therefore not calculated for the 2:1 complexes. In the optimized structures, the atomic charges were obtained by a Mulliken population analysis.

The molecular dynamics (MD) simulations were performed using AMBER4.1,[28] based on the following empirical representation of the potential energy, described in ref 28:

$$V = \sum_{\text{bonds}} K_r (r - r_{eq})^2 + \sum_{\text{angles}} K_\theta (\theta - \theta_{eq})^2 + \sum_{\text{dihedrals}} V_n (1 + \cos n\phi) + \sum_{i<j} (q_i q_j / R_{ij} - 2\epsilon_{ij} (R_{ij}^*/R_{ij})^6 + \epsilon_{ij} (R_{ij}^*/R_{ij})^{12})$$

We used the AMBER parameters[29] on the solute and atomic charges taken from the QM ab initio studies. The parameters of the UO_2^{2+} and NO_3^- are those of ref 12. The solute was immersed in a cubic box of TIP3P[30] water molecules, represented with periodic boundary conditions (see Table 5, vide infra). All nonbonded interactions were calculated using a residue based cutoff of 12 Å. After energy minimization, the dynamics was run for 100 ps at 300K and constant pressure of 1 atm.

The differences in free energies of hydration between states A (electronic distribution of OPR_3 and of $UO_2(NO_3)_2$ before complexation) and B (electronic distribution in the complex) were obtained using the statistical perturbation theory,[31] where the atomic charge of each atom i was calculated as $q_{i(\lambda)} = \lambda q_{i(B)} + (1 - \lambda) q_{i(A)}$, and λ was increased from 0 (state A) to 1 (state B) in 10 windows. At each window, we performed 1 ps of equilibration + 4 ps of data collection and the change in free energy ΔG_λ was obtained by

$$\Delta G_\lambda = RT \,\text{Ln}\, \langle \exp(E_\lambda - E_{\lambda+\Delta\lambda})/RT \rangle_\lambda$$

and $\Delta G = \sum_\lambda \Delta G_\lambda$.

The analysis of the trajectories was performed using out MDS and DRAW programs.[32]

TABLE 1: Total Energies, Orbital Energies, Structures, and Mulliken Charges Obtained at the HF/DZP* Level for the Free OPR_3 Ligands

R	H	Me	Ph
	Energies (au)		
E_T	−417.2928	−534.4057	−1105.7547
π^* P═O	0.199	0.211	0.276
σ^* P−O	0.181	0.199	0.235
π P═O	−0.438	−0.402	−0.409
σ P−O	−1.301	−1.273	−1.277
	Structures (Å and degrees)		
P═O	1.502	1.509	1.510
P−X[a]	1.411	1.822	1.824
O═P−X[a]	116.2	112.9	111.4
	Mulliken Charges[b]		
OPR_3 O	−0.600	−0.648	−0.640
	(−0.747)	(−0.800)	(−0.801)
P	0.414	0.564	0.472
	(0.792)	(0.746)	(0.843)
R	0.062	0.028	0.056
	(−0.015)	(0.018)	(−0.014)

[a] X = H in OPH_3 and X = C in $OPMe_3$ and $OPPh_3$. [b] Values in parentheses correspond to the HF/DZA*//HF/DZP* calculations.

Results

In the following sections 1−3, we describe the main structural and energy results in the gas phase, based on QM ab initio calculations. Unless otherwise specified, they were performed at the HF/DZP* level, common to all systems. Then, in section 4, we consider the effect of changes in solvation, due to the ER induced by complexation.

(1) QM ab Initio Calculations on the Free OPR_3 Ligands: Structures and Electronic Features. The main structural and electronic features of the free ligands (Table 1) obtained at the HF/DZP*//HF/DZP* level show that the phosphoryl groups of the alkyl and phenyl derivatives are very similar: see, for instance, the P═O distance, the q_o charge, and the energies of the π and σ oxygen lone-pair orbitals. These values differ in the smallest OPH_3 ligand, where the P═O bond is somewhat shorter, the oxygen lone-pair orbitals are more stable, and the q_o charge of the phosphoryl oxygen is less negative. Thus, the replacement of alkyl or aryl groups by H atoms for computer time saving purposes may lead to some artifacts. On the other hand, the similarity of phosphoryl groups next to aryl/alkyl ligands found in their free states contrasts with the differences observed in their complexed states (see next).

The calculated structures of $OPMe_3$ and $OPPh_3$ are in reasonable agreement with the ones determined either by electron diffraction (for $OPMe_3$[33]) or by X-ray crystallography (for $OPMe_3$ and $OPPh_3$).[34] Experimentally, the P═O and P−C bond lengths in $OPMe_3$ obtained by X-ray crystallography are somewhat different (1.489 and 1.771 Å) from those determined by electron diffraction data (1.476 and 1.809 Å). These values are close to those obtained also by crystallography for the $OPPh_3$ molecule (from 1.48 to 1.49 Å, and 1.80 Å).[34] Our calculated values amount to 1.51 and 1.82 Å at the HF/DZP* level. Thus the P═O bond is slightly too long. This feature is not corrected at the MP2 level, since the corresponding MP2/DZP* value is 1.54 Å (the P−C value being 1.84 Å). It is traced instead to the lack of polarization functions on the atoms other than phosphorus: For $OPMe_3$ the DZA* basis set, that includes such polarization functions, yields P═O and P−C values of 1.49 and 1.83 Å (HF level). We note that a previous calculation,[35] using for the phosphorus d polarization function an exponent that was optimized on the molecular system, led to slightly better values of 1.48 and 1.84 Å.

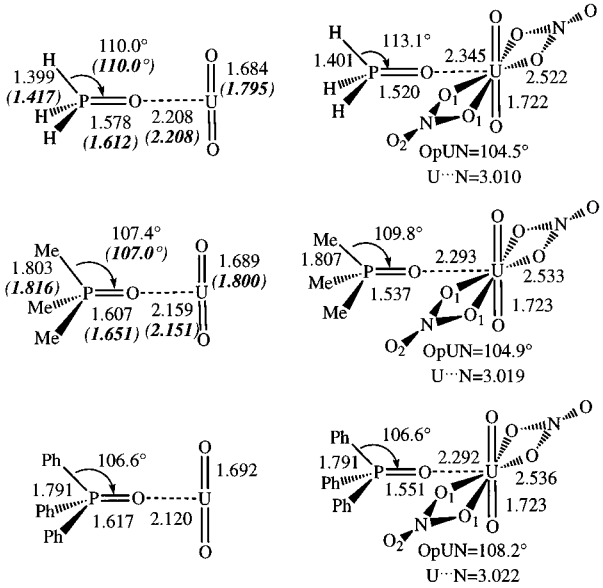

Figure 2. Optimized structural parameters in the $UO_2^{2+}\cdots OPR_3$ and $UO_2(NO_3)_2\cdots OPR_3$ 1:1 complexes with the DZP* basis set at the HF level (first line) and at the MP2 level (in parentheses).

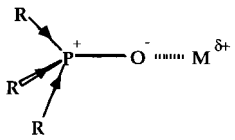

Figure 3. Schematic representation of stabilizing electronic rearrangements upon coordination of OPR_3 to UO_2^{2+}.

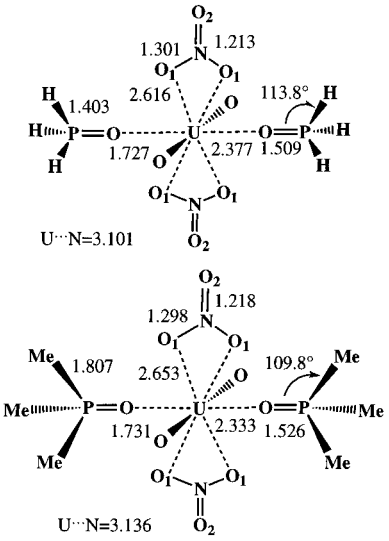

Figure 4. Optimized structural parameters in the $UO_2(NO_3)_2\cdots OPR_3$ 2:1 complexes (with the DZP* basis set at the HF level).

(2) Binding of OPR_3 to the UO_2^{2+}Cation and to the $UO_2(NO_3)_2$ Salt in the Gas Phase: ab Initio QM Results. The structures of the ab initio minimized complexes are reported in Figures 2−4, and the energy features, together with the Mulliken charges, are reported in Tables 2 and 3.

$UO_2^{2+}\cdots OPR_3$ Complexes (No Counterion). We first consider the $UO_2^{2+}\cdots OPR_3$ complexes and define the "complexation energy" as $\Delta E = E_{complex} - E_{OPR3} - E_{cation}$.

Table 2 shows that there is a spectacular substituent effect on the intrinsic ion$\cdots$$OPR_3$ attraction energies which increase from 122 (R = H) to 163 kcal mol^{-1} (R = Ph). As the BSSE correction is nearly constant in the series (from −4.0 to −4.5

TABLE 2: Total Energies (in au), Interaction Energies (in kcal mol^{-1}), and Mulliken Charges in the $UO_2^{2+}\cdots OPR_3$ 1:1 Complexes

	H			Me			Ph	
R level	HF/DZP*// HF/DZP*	HF/DZA*// HF/DZP*	MP2/DZP*// MP2/DZP*	HF/DZP*// HF/DZP*	HF/DZA*// HF/DZP*	MP2/DZP*// MP2/DZP*	HF/DZP*// HF/DZP*	HF/DZA*// HF/DZP*
				Energies				
E_T	−617.1248	−617.2071	−617.9999	−734.2754	−734.4100	−735.4156	−1305.6520	1306.0242
ΔE	−121.6	−108.4	−115.8	−145.3	−132.2	−143.1	−162.6	−149.2
BSSE	−4.0	−3.1	−7.9	−4.5			−4.5	
ΔE^{cp}	−117.6	−105.3	−107.9	−140.8			−158.1	
				Mulliken Charges				
UO_2 O	−0.121	−0.262		−0.146	−0.287		−0.178	−0.309
U	1.967	2.250		1.943	2.224		1.942	2.203
Total UO_2	1.725	1.726		1.651	1.650		1.586	1.585
OPR_3 O	−0.844	−0.923		−0.885	−0.968		−0.903	−0.991
P	0.465	0.792		0.549	0.691		0.555	0.927
R	0.218	0.135		0.228	0.209		0.254	0.159
Total OPR_3	0.275	0.274		0.349	0.350		0.414	0.415

TABLE 3: Total Energies (in au), Interaction Energies (in kcal mol^{-1}), and Mulliken Charges in the $UO_2(NO_3)_2\cdots OPR_3$ 1:1 and 1:2 Complexes (Calculations Performed with the DZP* Basis Set at the HF Level)

	H		Me		Ph
R	1:1	1:2	1:1	1:2	1:1
		Energies			
E_T (a.u.)	−1175.4582	−1592.8003	−1292.5869	−1827.0500	−1863.9342
ΔE	−49.3	−40.1 (ΔE_1)	−59.2	−47.6 (ΔE_1)	−58.1
		−30.9 (ΔE_2)		−36.0 (ΔE_2)	
BSSE	−4.5		−5.0		−5.2
ΔE^{cp}	−44.8		−54.2		52.9
		Mulliken Charges			
UO_2 O	−0.301	−0.341	−0.341	−0.360	−0.322
U	1.867	1.934	1.882	1.964	1.893
Total UO_2	1.265	1.252	1.258	1.244	1.249
OPR_3 O	−0.717	−0.671	−0.786	−0.732	−0.861
P	0.434	0.436	0.567	0.574	0.554
R	0.136	0.121	0.125	0.104	0.157
Total OPR_3	0.125	0.128	0.156	0.151	0.164
NO_3 N	0.521	0.506	0.520	0.504	0.523
O_1	−0.497	−0.493	−0.498	−0.494	−0.499
O_2	−0.222	−0.274	−0.231	−0.289	−0.232
Total NO_3	−0.695	−0.754	−0.707	−0.773	−0.707

kcal mol^{-1}), the BSSE corrected complexation energies ΔE^{cp} follow the same trend as ΔE, and the energies range from −118 (OPH_3) to −141 ($OPMe_3$) and −158 kcal mol^{-1} ($OPPh_3$). The interaction energies increase with the polarizability of R ($\alpha_H < \alpha_{alkyl} < \alpha_{aryl}$[36,37]) which varies as the electron donating properties of R. The evolution of structural and electronic features may be understood if one considers the ionic form $^-O-PR_3$ of PR_3 (Figure 3), which is stabilized by R-donating groups (Ph > alkyl > H) and displays the largest interactions with UO_2^{2+}.

Indeed, in the H/Me/Ph series of complexes, the $U\cdots O_P$ distance shortens (from 2.21 to 2.12 Å), while O═P increases (from 1.58 to 1.62 Å). This is consistent with the weakening of P═O stretching frequencies upon complexation observed by IR.[38] The phosphoryl oxygen becomes more negative (from −0.84 to −0.90 e). There is also a significant electron transfer (from 0.27 to 0.41 e) from the ligand to UO_2^{2+}. A comparison of the $OPMe_3$/$OPPh_3$ complexes reveals that the electrons are transferred to the O atoms of UO_2^{2+}, while the q_U charge remains constant. In agreement with the above scheme, the q_P charge is less positive in the $OPPh_3$ than in the $OPMe_3$ complex. Comparison of the charge distribution in the free/complexed ligands (Tables 1 and 2) shows in every case a clear $R^{\delta+}-PO^{\delta-}$ polarization of the ligand induced by the complexation.

Methodological tests concerning the role of polarization functions in the basis set were performed on the three OPR_3 complexes. A comparison of the HF/DZA*//HF/DZP* with the HF/DZP*//HF/DZP* interaction energies ΔE shows a decrease (from 13.1 to 13.4 kcal mol^{-1}) with the more extended DZA* basis set (Table 2). However, as this energy shift is nearly independent of R, the *relative* binding energies of the OPH_3/$OPMe_3$/$OPPh_3$ ligands are not critically dependent on the use of polarization functions on C, O, and H atoms. Thus the DZP* basis set was used for the other complexes.

One may also worry about the role of electron correlation on the ion−ligand interaction energies ΔE. To this end we compared HF to MP2 calculations for the OPH_3/$OPMe_3$ complexes with the DZP* basis set (Table 2). Taking into account the correction for electron correlation somewhat reduces ΔE (by 5.9/2.1 kcal mol^{-1}, respectively) but this effect is relatively small, compared to the change related to the R substituent (about 20 kcal mol^{-1}).

$UO_2(NO_3)_2\cdots OPR_3$ Complexes. We now consider the $UO_2(NO_3)_2\cdots OPR_3$ 1:1 complexes and define the complexation energy as $\Delta E = E_{complex} - E_{OPR3} - E_{salt}$, where the $UO_2(NO_3)_2$ salt and OPR_3 ligand have been energy minimized. The BSSE energy correction is again nearly constant in this series (from 4.5 to 5.2 kcal mol^{-1}; see Table 3), and it will not be considered further. For the two smallest OPH_3 and $OPMe_3$ ligands, the 2:1 stoichiometries were also calculated. Their ΔE_1 and ΔE_2

energies correspond to the successive complexation of the first and second ligand, respectively.

For the 1:1 complexes, it can be first noticed that, upon NO_3^- coordination to the uranyl cation, the interaction energy with OPR_3 drops markedly and that it depends on the R substituent (Δ = 72 kcal mol^{-1} for OPH_3, 86 kcal mol^{-1} for $OPMe_3$, and 104 kcal mol^{-1} for $OPPh_3$). These numbers suggest that there is some repulsion between the NO_3^- anions and OPR_3, which increases from OPH_3 to $OPPh_3$. Second, concerning the effect of R on the complexation energy ΔE, the OPH_3 ligand is the least well complexed, as when there are no counterions. There is, however, a marked difference concerning the $OPMe_3$/$OPPh_3$ ligands, which now display similar interactions with the $UO_2(NO_3)_2$ fragment (about 58 kcal mol^{-1}). Thus, the most polarizable and electron donating Ph group no longer leads to the most stable complex. We believe that this is related to the anion−ligand repulsions (see below). The structural consequence of these repulsions is that, in the 1:1 complexes, the angle between the $O_P\cdots U\cdots N_{NO_3^-}$ atoms deviates from 90° and is largest for the $OPPh_3$ complex (108°). The $U\cdots N_{NO_3^-}$ distance is also largest in that complex (Figure 2), and is 0.05 Å larger than in the isolated $UO_2(NO_3)_2$ salt. Another related parameter is the change of $U\cdots O_P$ distances. In the complexes without counterions, the latter decreases from $OPMe_3$ to $OPPh_3$, in relation with the increase of cation−ligand interactions. In the presence of NO_3^- counterions, this distance is nearly identical in these two complexes; presumably as a compromise between antagonist forces: compared to $OPMe_3$, the $OPPh_3$ ligand is more attracted by the cation, but is also more repulsed by the anions.

Some other interesting differences dealing with the structure of UO_2^{2+} can be noticed: in the absence of counterions, $d_{U=O}$ increases from 1.68 (OPH_3) to 1.69 Å ($OPPh_3$). Anion coordination to the cation markedly lengthens the U═O bond, whose length remains constant whatever the ligand is (1.72 Å).

When the OPR_3 ligand binds the neutral $UO_2(NO_3)_2$ species, the electron transfer from the ligand is much weaker (from 0.13 to 0.16 e) than in the UO_2^{2+} complexes (from 0.27 to 0.41 e), but follows the same trend as a function of R. Conversely, the total charge of uranyl displays minor perturbations in the $UO_2(NO_3)_2$ complexes (from 1.26 to 1.25 e), compared to the UO_2^{2+} complexes (from 1.72 to 1.59 e), due to a compensation between the changes of q_O and q_U contributions (Table 3).

We now consider the 2:1 complexes which have been optimized with the OPH_3 and $OPMe_3$ ligands. First, as expected, the complexation of a second ligand brings about less stabilization (about 10 kcal mol^{-1}) than the first one, due to the ligand−ligand and to the ligand−anion repulsions. However, ΔE_2 follows the same trend as ΔE_1 (i.e., is more attractive with $OPMe_3$ than with OPH_3 (by about 6 kcal mol^{-1}). As a result of the ligand−ligand and ligand−anion repulsions, the $U\cdots O_P$ distances are larger in the 2:1 than in the 1:1 complexes (Δ = 0.17 Å with OPH_3 and 0.09 Å with $OPMe_3$ ligands). The P═O bonds of the ligand are also shorter in the 2:1 than in the 1:1 complexes (Δ = 0.07 Å with OPH_3 and 0.01 Å with $OPMe_3$ ligands).

Concerning the NO_3^- anions, it can be noticed that the two N−O distances of the coordinated oxygens are longer than that of the free N−O (by 0.08 to 0.10 Å), as found in related solid-state structures.[16]

(3) Binding of OPR_3 to the Sr^{2+} Cation and to the $Sr(NO_3)_2$ Salt in the Gas Phase: ab initio QM Results. The calculations on the $Sr^{2+}\cdots OPR_3$ and $Sr(NO_3)_2OPR_3$ 1:1 complexes were performed at the HF/DZP*//HF/DZP* level, assuming a coplanar arrangement of the $UO_2(NO_3)_2$ and P═O groups (local C_{2v} symmetry). Optimized structural parameters and related energy features are reported in Figure 5 and in Table 4. They follow the same trends as for the UO_2^{2+} cation complexes. First, the binding energy of OPR_3 increases in the series H < Me < Ph, without or with counterions, and is reduced upon coordination of NO_3^- counterions. However, interactions of a given ligand with Sr^{2+} are weaker than those with UO_2^{2+} (by about 24 to 35 kcal mol^{-1} without counterions, and by 15 to 19 kcal mol^{-1} with counterions). Accordingly, in the absence of counterions, the O_P distances with Sr^{2+} are 0.03−0.05 Å larger than those with the U atom of UO_2^{2+}. They also decrease from the OPH_3 to $OPPh_3$ by 0.07 Å. In line with this difference in ion−ligand interactions, the O═P bonds are 0.01 to 0.02 Å shorter in the Sr^{2+} than in the UO_2^{2+} complexes. The electron transfer from the ligand is also smaller in the Sr^{2+} (from 0.14 to 0.21 e) than in the UO_2^{2+} complexes (from 0.27 to 0.41 e). Similar trends are observed in $UO_2(NO_3)_2$ complexes, but the effects are smaller (see Table 3). Thus, to summarize this section, it is clear that, despite the lack of repulsive secondary interactions between the O_{UO_2} and O_P atoms, the spherical Sr^{2+} cation displays weaker interactions with phosphoryl ligands than the linear UO_2^{2+} ion does. This conclusion is confirmed by similar QM calculations on the corresponding 2:1 complexes $Sr(NO_3)_2(OPR_3)_2$.[45]

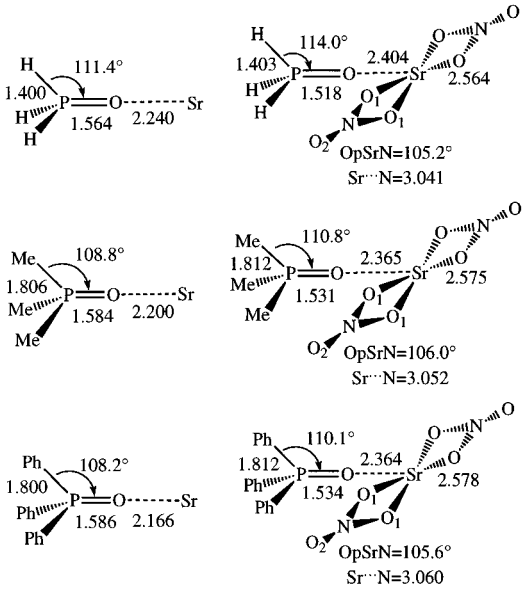

Figure 5. Optimized structural parameters in the $Sr^{2+}\cdots OPR_3$ and $Sr(NO_3)_2\cdots OPR_3$ 1:1 complexes (with the DZP* basis set at the HF level).

(4) Changes in Free Energies of Hydration upon Complexation-Induced Electronic Reorganization in the $UO_2(NO_3)_2\cdots OPR_3$ 1:1 and 2:1 Complexes. In this section, we attempt to get insights into changes in hydration free energies of the solute ΔG_{hyd}, due to the ER induced by complexation. For this purpose, we assume for simplicity that the ER in solution can be depicted by the ER in the gas phase (i.e., that the mutual solute−solvent polarization and charge-transfer interactions can be neglected). In these calculations, the potential energy of the system is depicted using a force field model, where the nonbonded interatomic interactions are calculated by a 1-6-12 Coulombic + Lennard-Jones potential.

TABLE 4: Total Energies (in au) and Interaction Energies (in kcal mol^{-1}), and Mulliken Charges in the $Sr^{2+}\cdots OPR_3$ and $Sr(NO_3)_2\cdots OPR_3$ 1:1 Complexes (Calculations Performed with the DZP* Basis Set at the HF Level)

$Sr^{2+}(NO_3^-)_n\cdots OPR_3$	$Sr^{2+}(NO_3^-)_n\cdots OPH_3$		$Sr^{2+}(NO_3^-)_n\cdots OPMe_3$		$Sr^{2+}(NO_3^-)_n\cdots OPPh_3$	
n	0	2	0	2	0	2
			Energies			
E_T (a.u.)	−447.2270	−1105.4811	−564.3673	−1122.6043	−1135.7363	−1693.9536
ΔE	−96.4	−33.8	−113.6	−40.3	−126.1	−40.5
BSSE	−3.1	−3.3	−3.3	−3.6	−2.6	−3.2
ΔE^{cp}	−93.3	−30.5	−110.3	−36.7	−123.5	−37.3
			Mulliken Charges			
Sr	1.855	1.568	1.807	1.542	1.788	1.552
OPR_3 O	−0.889	−0.700	−0.953	−0.769	−0.997	−0.816
P	0.446	0.423	0.570	0.574	0.588	0.528
R	0.196	0.121	0.192	0.103	0.207	0.130
Total OPR_3	0.145	0.086	0.193	0.114	0.212	0.102
NO_3 N		0.479		0.479		0.481
O_1		−0.525		−0.522		−0.522
O_2		−0.256		−0.263		−0.264
Total NO_3		−0.827		−0.828		−0.827

TABLE 5: MD and FEP Simulations on the $UO_2(NO_3)_2\cdots OPR_3$ 1:1 and 1:2 Complexes in Water. Size of the Water Box (Å^3) and Number of Water Molecules

R	stoichiometry	box size	N_{wat}
H	1:1	28.7 × 30.6 × 26.2	791
	1:2	31.5 × 31.2 × 26.3	884
Me	1:1	31.4 × 29.0 × 27.1	829
	1:2	32.8 × 31.7 × 26.8	957
Ph	1:1	33.6 × 30.7 × 31.1	1088
	1:2	36.2 × 32.2 × 31.7	1238

CHART 1: Thermodynamic Cycle Showing the Charge Mutations from Direct/Two Steps Charge Mutations within the Complexes

$$\begin{array}{ccc} OPR_3^A \quad UO_2(NO_3)_2^A & \xrightarrow{\Delta G^{Total}} & OPR_3^B \quad UO_2(NO_3)_2^B \\ \Delta G^{OPR_3} \downarrow & & \uparrow \Delta G^{salt} \\ OPR_3^B \quad UO_2(NO_3)_2^A & & \end{array}$$

The atomic charges come from a Mulliken analysis of the HF/DZP* wave functions of the isolated OPR_3 ligand and $UO_2(NO_3)_2$ salt (reference state A) and of the $UO_2(NO_3)_2\cdots OPR_3$ complex (state B). Calculation of changes in free energy by FEP requires adequate sampling of the system by MD. We noticed, as in our previous studies on nitrato complexes in water,[10,12,13] that the free MD led to changes in cation coordination: the NO_3^- anions evolve from a bidendate to a monodendate coordination, while some water molecules move in the first coordination sphere of the cation. It is not clear whether such coordination patterns, different from those observed in solid-state analogues,[16] result from computational artifacts or if they depict the real solution behavior. They are followed by large energy changes, which depend on the ligand (via changes in water accessibility and in nonbonded interactions). As our goal is to compare solvation effects due to electronic changes in the solute, from a ligand to the other, we decided to impose a common coordination type for the complexes in solution. For this purpose, a restraining harmonic potential $k(d_0 - d)^2$ was imposed to the four $U\cdots O_{NO_3^-}$ distances d to achieve a bidentate coordination of the anion (k = 20 kcal mol^{-1}; d_0 = 2.55 Å). This led to weak constraint energies (from 1.2 to 1.6 kcal mol^{-1}). All other parameters of the system were free of constraints during the simulations. In all cases, excepted for the OPH_3 2:1 complex, the ligands remained bound to the uranyl ion in water.

Two independent mutations were performed on the complexes (see Chart 1). In the first one (ΔG^{Total}), the charges of the whole solute were mutated simultaneously. In the second one, we calculated first the change in hydration free energy due the ER of the complexed OPR_3 ligand only (ΔG^{OPR_3}), followed by the contribution of the $UO_2(NO_3)_2$ moiety (ΔG^{salt}). The results are reported Table 6. One first notices that ΔG^{Total} is, within 1 kcal mol^{-1}, equal to the sum of ΔG^{OPR_3} and ΔG^{salt}, which indicates that the sampling is sufficient.

The results make clear that, in all cases, for the 1:1 and for the 2:1 complexes, the electronic reorganization of the solute which is induced by complexation enhances its solvation: ΔG^{Total} is negative, as are the ΔG^{OPR3} and ΔG^{salt} contributions. The most important and unexpected result is the near constancy of ΔG^{Total} when the ligand changes: ΔG^{Total} is about − 16 kcal mol^{-1} for the 2:1 complexes and −12 kcal mol^{-1} for the 1:1 complexes. This likely results from a compensation of two opposite effects: in the H/Me/Ph series of OPR_3 ligands, the charge transfer from the ligand to uranyl cation increases, and the latter should interact less with water. On the other hand, the OPR_3 ligand becomes more polarized by the cation, and should interact better with water. These trends are analyzed by an energy-component analysis performed on the complexes simulated by MD for 100 ps with the charges of state A and with those of state B. The average interaction energies between OPR_3, the $UO_2(NO_3)_2$ moiety, and water are reported in Table 6. They confirm that upon ER the $OPR_3\cdots$water attraction increases (by 15−19 kcal mol^{-1} for the 1:1 complexes, and by 7−9 kcal mol^{-1} in the 2:1 complexes), while the $UO_2^{2+}\cdots$water interactions decrease (by 5−17 kcal mol^{-1} in 1:1 complexes and by 5−12 kcal mol^{-1} in 2:1 complexes). The solvent-accessible surface of the different moieties and precise hydration patterns of the complex also play an important role. Indeed, in the 1:1 complexes, where the uranyl cation can coordinate one water molecule, the $UO_2^{2+}\cdots$ water interactions are attractive (from −35 to −7 kcal mol^{-1}, state B), whereas they are repulsive in the 2:1 complexes (from +7 to +48 kcal mol^{-1}, state B). The large variation in these numbers also point out the dramatic effect of the ligand substituents on the cation solvent interactions. Generally speaking, this should be important in modeling studies of transition metal complexes in polar solvents, when, for purpose of computer time savings, substituents are replaced by H or by small alkyl groups.

Another interesting feature emerges from the energy component analysis of Table 6: the cation−ligand interaction energies, although obtained from a relatively crude force field model, correctly reproduce the trends noticed above in the gas phase. With both sets of charges, the sequence of binding is OPH_3 < $OPMe_3$ < $OPPh_3$. As expected, the energy scale is larger with the charges of state B (about 34 ± 3 kcal mol^{-1} for

TABLE 6: Complexes in Water. Relative Free Energies of Hydration and Average Energy Components (kcal mol^{-1})

	1:1 complexes			1:2 complexes		
	R = H	R = Me	R = Ph	R = H	R = Me	R = Ph
$\Delta G^{\text{Total}\,a}$	-11.3 ± 0.4	-12.4 ± 0.4	-12.0 ± 0.6	-15.1 ± 0.1	-16.2 ± 0.4	-16.6 ± 0.4
$\Delta G^{\text{OPR}_3\,b}$	-8.2 ± 0.1	-8.4 ± 0.3	-5.9 ± 0.6	-8.9 ± 0.9 [f]	-7.8 ± 0.2	-7.5 ± 0.1
$\Delta G^{\text{salt}\,c}$	-3.1 ± 0.1	-4.6 ± 0.1	-5.3 ± 0.1	-7.1 ± 0.8 [f]	-8.7 ± 0.1	-10.4 ± 0.1
$\langle E(\text{Uranyl}\cdots\text{OPR}_3)\rangle \text{A}^d$	-40 ± 2	-51 ± 2	-63 ± 3	-40 ± 3	-52 ± 2	-64 ± 3
$\langle E(\text{Uranyl}\cdots\text{OPR}_3)\rangle \text{B}^e$	-39 ± 3	-51 ± 3	-74 ± 3	-35 ± 3	-48 ± 3	-68 ± 2
$\langle E(\text{OPR}_3\cdots\text{Wat})\rangle \text{A}^d$	-11 ± 5	-15 ± 5	-43 ± 6	-17 ± 4	-20 ± 5	-52 ± 7
$\langle E(\text{OPR}_3\cdots\text{Wat})\rangle \text{B}^e$	-28 ± 6	-30 ± 7	-62 ± 10	-26 ± 5	-30 ± 7	-59 ± 7
$\langle E(\text{Uranyl}\cdots\text{Wat})\rangle \text{A}^d$	-40 ± 10	-35 ± 10	-24 ± 10	-1 ± 11	$+9 \pm 11$	$+27 \pm 10$
$\langle E(\text{Uranyl}\cdots\text{Wat})\rangle \text{B}^e$	-35 ± 11	-25 ± 11	-7 ± 11	$+7 \pm 10$	$+18 \pm 11$	$+48 \pm 11$

[a] Calculated by mutating the charges of the whole complex. [b] Calculated by mutating the charges of OPR_3 within the complex (step 1). [c] Calculated by mutating the charges of $UO_2(NO_3)_2$ within the complex (step 2). [d] Average interaction energies and fluctuations in the complex, calculated with the charges of OPR_3 and $UO_2(NO_3)_2$ uncomplexed (state A). [e] Average interaction energies and fluctuations in the complex, calculated with the charges of the OPR_3 and $UO_2(NO_3)_2$ within the complex (state B). [f] One OPH_3 ligand dissociates during the simulation.

1:1 and 2:1 complexes) than with those of state A (about 24 ± 3 kcal mol^{-1} for 1:1 and 2:1 complexes). These numbers are smaller than those calculated in the gas phase because the U···O distances are somewhat longer and looser in solution than they are in the gas phase. It is however gratifying to note, as did Craw et al.,[7] that force-field calculations provide similar trends for uranyl···ligand interactions, as those obtained from QM studies alone.

Discussion and Conclusion

We report theoretical studies on complexes of both practical and theoretical importance. The QM calculations allow to get insights into the gas-phase (intrinsic) binding features. As expected from polarization and charge-transfer effects, aryl substituted phosphine oxide ligands interact better with UO_2^{2+} than alkyl analogues do. The same conclusion holds with the Sr^{2+} or with the highly charged lanthanide or actinide cations.[39] However, multiple coordination of ligands and counterions to UO_2^{2+} may change this conclusion, as shown on the $UO_2(NO_3)_2$ complexes. A first effect, widely exploited in supramolecular chemistry, concerns the ligand−ligand repulsions around the ion. With macrocylic or polydentate ligands, such repulsions are already paid for in the course of the synthesis, instead of being paid for upon complexation.[18] This effect largely contributes to the "macrocyclic effect".[18] In our case, it is found that the "best" phosphorylated ligand bears aryl substituents, which are also the bulkiest and most repulsed by the NO_3^- counterions. The electrostatic repulsion increases with the ligand size and polarizability. In the optimized 1:1 complexes, we estimated these electrostatic interactions, using the ab initio HF/DZP*-optimized geometries and the Mulliken point charges within the complex. Indeed, the repulsion between the two NO_3^- anions and OPR_3 is larger with $OPPh_3$ than with the $OPMe_3$ ligand (19.5 and 25.1 kcal mol^{-1}, respectively). Using the charges from the DZA* calculations give the same trends (22.5 and 22.6 kcal mol^{-1}, respectively). Generally speaking, polarization of the ligand and of the anion, an intrinsic stabilizing feature, also increases the ligand−ligand and the ligand−anion repulsions. On the basis of these features, the importance of topologically connected binding sites of the ligand, as achieved in macrocyclic ionophores, can be stressed.

Another comment relates to the relevance of solid-state structures to study the coordination pattern of uranyl. To our knowledge, the data reported so far for complexes of monodentate ligands with NO_3^- [16] (or RCO_2^-) as counterions are of 2:1 instead of 1:1 stoichiometry. Our calculations clearly show that the precise structure and charge distribution depend on the stoichiometry and on the presence of counterions, and that the 1:1 complexes cannot be compared with the 2:1 ones. Thus, with macrocyclic ligands, like CMPO or phosphine oxyde derivatives of calixarenes,[19] it can be stressed that the competition between ligand wrapping around the cation and counterion coordination, markedly determines the binding efficiency and selectivity: suitable ligands replace not only the solvent (generally water) molecules coordinated to the cation, but also the counterions. This enhances the cation···binding sites interactions within the complex.

(1) Stereochemical Preference for OPR_3 Coordination to UO_2^{2+}. Two structural features deserve some comments. The first one concerns the linearity of the U···O═P unit, and the second the eclipsed/staggered arrangement of the R groups of OPR_3 with respect to the O═U═O axis of UO_2^{2+}. In the calculations reported above on the UO_2^{2+} complexes, the U···O═P unit was supposed to be linear ($\alpha = 180°$; see Figure 1) and kept fixed for time saving purposes, while one R group of OPR_3 was eclipsed with one U═O bond ($\gamma = 0°$; see Figure 1). Charge transfer and polarization effects are expected to be largest when α is 180°. In solid-state structures, however, this angle is not linear and close to 160° (see for instance the $(OPPh_3)_2UO_2X_2$ 2:1 complexes, with $X^- = Cl^-$ [40] or $X^- = NO_3^-$ [41]). This may be related to the $OPR_3\cdots X^-$ repulsions or to crystal environment effects. In the AMBER MD simulations on the 2:1 $UO_2(NO_3)_2\cdots OPPh_3$ complex in water, where the ligand was free to move, we found a U···O═P angle of 148° in the $OPPh_3$ 2:1 complex, which suggests that the linear arrangement is not optimal, due to steric interactions. In the solid-state structures of $UO_2(NO_3)$ complexed with CMPO ligands which possess a phosphoryl and a carbonyl group as potential binding sites, coordination to the U atom is not linear either. The U···O═P angles range from about 135° (corresponding to a bidentate coordination to both groups[42,43]) to 165° (corresponding to a monodentate coordination to O_P only[44]).

We therefore decided to perform additional QM calculations. We considered a staggered arrangement ($\gamma = 0°$; see Figure 1) of the $[UO_2\cdots OPR_3]^{2+}$ system and reoptimized the U···O, O═P distances, the U···O−P bond angle, and the rotation around the P−C bond. This yielded energies which were similar to those of the eclipsed form in the case of R = H or Me, and slightly higher in the case of R = Ph. Moreover, the optimized U···O−P α angle was always found very close to 180°. Enforcing then a value of 160° for this angle led to an additional destabilization of 7.7, 3.5, and 2.2 kcal mol^{-1} for R═H, Me, and Ph, respectively. We can thus conclude that the bent M−OPR_3 arrangement that is observed experimentally is not an *intrinsic* property of the OPR_3 complex, but is most probably due, in the $OPPh_3$ case, to the presence of other ligands and of

the counterions, or to some crystal packing effects. Indeed similar calculations carried out for the 1:1 $UO_2(NO_3)_2\cdots OPH_3$ and $UO_2(NO_3)_2\cdots OPMe_3$ complexes in which the $O_P\cdots U\cdots N_{NO3}$ angles were allowed to relax led also to a preference for a linear U···O−P arrangement, whatever the conformation of OPR_3, staggered or eclipsed with respect to O═U═O, is. On the other hand, for the staggered $UO_2(NO_3)_2\cdots OPPh_3$ system an optimized α angle of 169.3° was computed, leading to an energy stabilization of 1.7 kcal mol^{-1}, compared to the linear arrangement. Moreover, in two additional single point calculations on this system with the two O···U···N angles constrained at 90°, as in the 2:1 complexes, the structure with $\alpha = 160°$ was found to be destabilized by 20.4 kcal mol^{-1} with respect to the structure with $\alpha = 180°$. Finally in an attempt to check whether the above findings could also be applicable to the 2:1 complexes, geometry optimizations, limited again to the $U\cdots O_P$, $U\cdots O_{NO3}$, O═P, and U···N distances, the U···O−P bond angle and the rotational angle around the P−C bonds, were performed for $UO_2(NO_3)_2(OPH_3)_2$ and $UO_2(NO_3)_2(OPMe_3)_2$ (under C_i symmetry). As for the 1:1 systems, a linear geometry of the U···O−P unit and a free rotation of the OPR_3 ligand were found. Thus all these results taken together justify our choice of initial structures to compare the interactions of OPH_3, $OPMe_3$, and $OPPh_3$, in the gas phase and in solution. They also confirm the importance of anion−ligand interactions in complexes of the most bulky $OPPh_3$ ligands.

(2) Solvation and Binding Selectivity. Solvation is known to markedly modify the effectiveness of noncovalent interactions and of the complexation processes. An important aspect concerns the change in solvation energy upon complexation, most of which arises from the desolvation of the ion. Here, we consider another feature: upon complexation, there is a significant electronic reorganization ER, due mostly to charge transfer and polarization effects. Such ER induces a change in solvation free energies, which become more negative in the systems studied. In the series of OPR_3 ligands considered here, this change is found to be nearly constant, which indicates that this effect does not contribute markedly to their binding *selectivity*. At a quantitative level, this conclusion may depend on the electrostatic representation of the system (point charges/multipoles, etc.), as well as on the method used to derive these parameters. One might argue that ER is somewhat underestimated with Mulliken charges, as compared to ESP charges which are known to enhance the polarity of the system. We notice however that the dipole moments calculated with the Mulliken charges are close to those obtained from *ab initio* QM wave function (e.g., 4.9/4.7 D for OPH_3 free; 12.6/12.6 D for the OPH_3 complex; 7.9/5.1 D for $OPPh_3$ free, and 16.6/15.3 D for the $OPPh_3$ complex). We attempted to derive such charges using the Merz Kollman procedure, but they led to some inconsistencies concerning the phosphoryl bond polarity, due to the poor solvent accessibility of this group within the complex. They are reported in ref 45. Generally, in MD and FEP calculations, the point charges on the ligand are kept fixed. Merz et al. studied the PMF of K^+ dissociation from 18-crown-6 in methanol and recalculated ESP charges along the PMF.[46] Mixed QM/MM methods, where the ligand is calculated by QM and the rest of the system by classical MM methods represent a promising approach to analyze such effects.[47−50] Improved treatments should also take into account the ER of the first shell solvent molecules.[49] Our study with a fixed solvent representation shows that the change in free energy due to ER is quite large (about 11 to 16 kcal mol^{-1}) compared to energy differences related to the binding selectivities. As pointed out by the energy component analysis of aqueous solutions simulated by mixed MM/QM methods, solute−solvent polarization energies should be also taken into account.[47,50] We chose water as solvent to model a polar protic solvent which displays significant interactions with polar solutes, but as far as liquid−liquid extraction processes are concerned, it is clear that the change in solvation energy due to the ER depends markedly on the microenvironment of the complexed cation, including the whole ligand, the counterions, and the water molecules dragged in the organic phase. These questions are presently investigated by simulations in our laboratory.

Acknowledgment. The authors are grateful to PRACTIS for supporting part of this work and to IDRIS for computer resources. F. Hutschka thanks the French ministry of research for a grant. We are also grateful to Professor P. J. Hay for providng us pseudopotential parameters of U. U. L. Troxler thanks EEC for a grant (Grant F14W-CT0022).

References and Notes

(1) Rozen, A. M. *J. Radioanal. Nucl. Chem.* **1990**, *143*, 337−355.
(2) Cecille, L.; Casarci, M.; Pietrelli, L. *New separation chemistry techniques for radioactive waste and other specific applications*; Commission of the European Communities; Elsevier Applied Science: New York, 1991.
(3) Franczyk, T. S.; Czerwinski, K. R.; Raymond, K. N. *J. Am. Chem. Soc.* **1992**, *114*, 8138−8146.
(4) Tabushi, I.; Kokube, Y. *Nippon Kaisui Gakkaishi* **1982**, *36*, 205.
(5) Badertscher, M.; Welti, M.; Portmann, P.; Pretsch, E. *Top. Curr. Chem.* **1986**, *136*, 17 and references therein.
(6) Cornehl, H. H.; Heineman, C.; Marçalo, J.; de Matos, A. P.; Schwarz, H. *Angew. Chem., Int. Ed. Engl.* **1996**, *35*, 891−894 and references therein.
(7) Craw, J. S.; Vincent, M. A. *J. Phys. Chem.* **1995**, *99*, 10181−10185.
(8) Pyykkö, P.; Zhao, Y. *Inorg. Chem.* **1991**, *30*, 3787.
(9) van Wezenbeck, E. M.; Baerends, E. J.; Snijders, J. G. *Theor. Chim. Acta* **1991**, *81*, 129.
(10) Guilbaud, P.; Wipff, G. *J. Phys. Chem.* **1993**, *97*, 5685−5692.
(11) Guilbaud, P.; Wipff, G. *J. Mol. Recognit. Inclusion Phenom.* **1993**, *16*, 169−188.
(12) Guilbaud, P.; Wipf, G. *J. Mol. Struct. (THEOCHEM)* **1996**, *366*, 55−63. Guilbaud, P.; Wipff, G. *New J. Chem.* **1996**, *20*, 631−642.
(13) Muzet, N.; Wipff, G.; Casnati, A.; Domiano, L.; Ungaro, R.; Ugozzoli, F. *J. Chem. Soc., Perkin Trans. 2* **1996**, 1065−1075.
(14) Horwitz, E. P.; Diamond, H.; Martin, K. A. *Solvent Ext. Ion Exch.* **1987**, *5*, 447−470.
(15) Choppin, G. R.; Nach, K. L. *Radiochim. Acta* **1995**, *70/71*, 225−236.
(16) Casellato, U.; Vigato, P. A.; Vidali, M. *Coord. Chem. Rev.* **1981**, *36*, 183−265.
(17) Izatt, R. M.; Bradshaw, J. S.; Nielsen, S. A.; Lamb, J. D.; Christensen, J. J.; Sen, D. *Chem. Rev.* **1985**, *85*, 271−339.
(18) Lehn, J. M. *Struct. Bonding* **1973**, *161*, 1−69.
(19) Arnaud-Neu, F.; Böhmer, V.; Dozol, J. F.; Grüttner, C.; Jakobi, R. A.; Kraft, D.; Mauprivez, O.; Rouquette, H.; Schwing-Weill, M.-J.; Simon, N.; Vogt, W. *J. Chem. Soc., Perkin Trans. 2* **1996**, 1175. Yaftian, M. R.; Burgard, M.; Matt, D.; Dieleman, C. B.; Rastegar, F. *Solvent Extract. Ion Exch.* **1997**, *15*, 975−989.
(20) Frisch, M. J.; Trucks, G. W.; Head-Gordon, M.; Gill, P. M. W.; Wong, M. W.; Foresman, J. B.; Johnson, B. G.; Schlegel, H. B.; Robb, M. A.; Reploge, E. S.; Gomperts, R.; Andres, J. L.; Raghavachari, K.; Binkley, J. S.; Gonzales, C.; Martin, R. L.; Fox, D. J.; Defrees, D. J.; Baker, J.; Stewart, J. J. P.; Pople, J. A. *Gaussian-92*; Gaussian, Inc.: Pittsburgh, PA, 1992.
(21) Hay, P. J. Private communication.
(22) Dolg, M. Lanthanide and Actinides. in *Encyclopedia of Computational Chemistry*; Schleyer, P. v. R.; Ed.; J. Wiley: New York. In press.
(23) Pyykkö, P.; Li, J.; Runeberg, N. *J. Phys. Chem.* **1994**, *98*, 4809.
(24) Küchle, W.; Dolg, M.; Stoll, H.; Preuss, H. *J. Chem. Phys.* **1994**, *100*, 7535.
(25) Dalley, N. K.; Mueller, M. H.; Simonsen, S. H. *Inorg. Chem.* **1971**, *10*, 323−328.
(26) Taylor, J. C.; Mueller, M. H. *Acta Crystallogr.* **1965**, *19*, 536−543.
(27) Boys, S. F.; Bernardi, F. *Mol. Phys.* **1970**, *19*, 553.

(28) Pearlman, D. A.; Case, D. A.; Cadwell, J. C.; Seibel, G. L.; Singh, U. C.; Weiner, P.; Kollman, P. A. *AMBER4*; University of California: San Francisco, 1991.
(29) Cornell, W. D.; Cieplak, P.; Bayly, C. I.; Gould, I. R.; Merz, K. M.; Ferguson, D. M.; Spellmeyer, D. C.; Fox, T.; Caldwell, J. W.; Kollman, P. A. *J. Am. Chem. Soc.* **1995**, *117*, 5179−5197.
(30) Jorgensen, W. L. *J. Am. Chem. Soc*. **1981**, *103*, 335−340.
(31) Bash, P. A.; Singh, U. C.; Langridge, R.; Kollman, P. A. *Science* **1987**, *236*, 564−568.
(32) Engler, E.; Wipff, G. *MD-DRAW software. Display of dynamic structures from MD simulations.* In *Crystallography of Supramolecular Compounds*; Tsoucaris, G., Ed.; Kluwer Academic Publishers: Dordrecht, 1996; pp 471−476.
(33) Wilkins, C. J.; Hagen, K.; Hedberg, L.; Shen, Q.; Hedberg, K. *J. Am. Chem. Soc.* **1975**, *97*, 6352−6358.
(34) Gilheany, D. G. *Chem. Rev.* **1994**, *94*, 1339−1374 and references therein.
(35) Bollinger, J. C.; Houriet, R.; Kern, C. W.; Perret, D.; Weber, J.; Yvernault, T. *J. Am. Chem. Soc.* **1985**, *107*, 5352−5358.
(36) Kollman, P. *J. Am. Chem. Soc.* **1977**, *99*, 4875.
(37) Morokuma, K. *Acc. Chem. Res.* **1977**, *10*, 294.
(38) Gans, P.; Smith, B. C. *J. Chem. Soc.* **1964**, 4172−4176.
(39) Troxler, L.; Dedieu, A.; Hutschka, F.; Wipff, G. *J. Mol. Struct. (THEOCHEM)* **1998**, *431*, 151−163.
(40) Bombieri, G.; Forsellini, E.; Day, J. P.; Azeez, W. I. *J. Chem. Soc., Dalton Trans.* **1978**, 677−680.
(41) Alcock, N. W.; Roberts, M. M.; Brown, D. *J. Chem. Soc., Dalton Trans.* **1982**, 25−31.
(42) Caudle, L. J.; Duesler, E. N.; Paine, R. T. *Inorg. Chim. Acta* **1985**, *110*, 91−100.
(43) Bowen, S. M.; Duesler, E. N.; Paine, R. T. *Inorg. Chem.* **1983**, *22*, 286−290.
(44) Babecki, R.; Platt, A. W. G.; Tebby, J. C.; Fawcett, J.; Russel, D. R. *Polyhedron* **1989**, *10*, 1357−1360.
(45) Hutschka, F. Thesis, Université Louis Pasteur, Strasbourg, 1997.
(46) Marrone, T. J.; Hartsough, D. S.; Merz, K. M., Jr. *J. Phys. Chem.* **1994**, *98*, 8, 1341−1343.
(47) Thompson, M. A.; Glendening, E. D.; Feller, D. *J. Phys. Chem.* **1994**, *98*, 10465−10476.
(48) Thompson, M. A. *J. Am. Chem. Soc.* **1995**, *117*, 11341−11344.
(49) Gao, J. *Acc. Chem. Res.* **1996**, *29*, 298−305.
(50) Gao, J. *J. Comput. Chem.* **1997**, *18*, 1061−1072.